The imaging features and clinical associations of a novel tau PET tracer - 18F-APN1607(18F-PM-PBB3) in Alzheimer's disease

Jung Lung Hsu
Chang Gung University https://orcid.org/0000-0001-6422-8870
Kun-Ju Lin
Chang Gung Memorial Hospital
Ing-Tsung Hsiao
Chang Gung University
Kuo-Lun Huang
Chang Gung Memorial Hospital
Chi-Hung Liu
Chang Gung Memorial Hospital
Hsiu-Chuan Wu
Chang Gung Memorial Hospital
Yi-Ching Weng
Chang Gung Memorial Hospital
Chu-Yun Huang
Taipei Medical University College of Pharmacy
Chiung-Chih Chang
Chang Gung Memorial Hospital Kaohsiung Branch
Tzu-Chen Yen
APRINOIA Therapeutic
Makoto Higuchi
NIRS
Ming-Kuei Jang
APRINOIA Therapeutic
Chin-Chang Huang (cch0537@adm.cgmh.org.tw)
Chang Gung Memorial Hospital

Research

Keywords: 18F-APN1607(18F-PM-PBB3), tau, Alzheimer' disease, positron emission tomography

Posted Date: March 9th, 2020

DOI: https://doi.org/10.21203/rs.3.rs-16387/v1

Abstract

Background: In vivo tau positron emission tomography (PET) imaging could help clarify the spatial distribution of tau deposition in Alzheimer's disease (AD) and aid in the differential diagnosis of tauopathies. To date, there have been no in vivo 18 F-APN1607 tau PET studies in patients with AD.

Methods: We applied tau tracer in twelve normal controls (NCs) and ten patients in the mild to moderate stage of probable AD. Detailed clinical information, cognitive measurements and disease severity were documented. Regional standardized uptake value ratios (SUVRs) from 18 F-AV-45 (florbetapir), 18 F-APN1607 PET images and regional gray matter (GM) atrophic ratios were calculated for further analysis.

Results: Quantitative analyses showed significantly elevated SUVRs in the frontal, temporal, parietal, occipital lobes, anterior and posterior cingulate gyri, precuneus, and parahippocampal region (all ps < 0.01) with medium to large effect sizes (0.44 - 0.75). The SUVRs from 18 F-APN1607 PET imaging showed significant correlations with the ADAS-cog scores (all ps < 0.01) and strong correlation coefficients (R squared ranged from 0.54 to 0.68), even adjusted for age and gender effects. Finally, the SUVRs from 18 F-APN1607 PET imaging of the parahippocampal region showed rapid saturation as the ADAS-cog scores increased, and the SUVRs of the posterior cingulate gyrus and the temporal, frontal, parietal and occipital regions slowly increased. The combined SUVRs from 18 F-AV-45 PET, 18 F-APN1607 PET and regional GM atrophic ratio showed that uptake associated with the amyloid burden rapidly increased and reach a plateau, whereas uptake associated with tau depositions increased slowly and finally followed by regional GM atrophic ratios in most regions as the ADAS-cog scores increased. However, different regions exhibited various combinations of these patterns.

Conclusions: Our findings suggest that the 18 F-APN1607 tau tracer showed a clear background without significant uptake in the basal ganglia or midbrain. Uptake of this tracer correlated well with cognitive changes and demonstrated the spatial pattern of amyloid, tau deposition and GM atrophy in the progression of AD. Thus, the regional base of dynamic biomarker changes was observed in the current study.

Trial registration: registration number (NCT03625128), date of registration(August 10, 2018), retrospectively registered.

Background

Tau protein is one of the important neuropathological substrates in the neurodegenerative diseases. The term "tauopathy" collectively refers to neurodegenerative disorders characterized by the pathological accumulation of tau protein, such as Alzheimer's disease (AD), frontotemporal dementia and others[1–3]. Recent advances in the selective tau tracers for positron emission tomography (PET) imaging allow in vivo exploration of the presence and extent of tau pathology in these patients[4]. Clinically, tau PET imaging can provide valuable support in the early differential diagnosis of neurodegenerative disorders by revealing whether a characteristic distribution of tau deposition is present[5].

Over the last few years, several tau tracers have developed in the living human brain, including the first-generation tau trace such as ^{18}F-AV-1451[6, 7], ^{18}F-THK-5117, ^{18}F-THK-5317, and ^{18}F-THK-5351[8–11], and the novel second-generation tau tracers, such as ^{11}C-PBB3, ^{18}F-RO69558948, ^{18}F-MK6240 and ^{18}F-PI2620 [12–14].

The first generation tau traces had several limitations, for example, 'off-target' binding; that is, the signal from tau tracers are due to monoamine oxidase B (MAO-B) binding [15]. ^{18}F-AV-1451 studies also showed the influence of signals on monoamine oxidase A(MAO-A) binding in vitro [16, 17].Other conditions that include astrocytosis in their histology may also show increased uptake of ^{18}F-THK-5351, as in the affected area in the semantic variant of primary progressive aphasia or in the ischemic-related regions in patients with vascular cognitive impairment[18, 19]. Furthermore, most of these tracers have shown high binding affinity in the deep brain nucleus, which is not a region where pathological studies show a high density of tangles in AD [20]. Thus, a tau imaging agent with low off-target binding in the brain remains an unmet need in the field of dementia research [5].

PBB3 is a tau tracer developed in 2014. After preclinical evaluation, ^{11}C-PBB3 has been demonstrated to effectively visualize tau pathology in patients with AD and non-AD tauopathies[12, 21]. Notably, the high-level retention of ^{11}C-PBB3 in the AD hippocampus, wherein tau pathology is enriched, sharply contrasted with the low hippocampal retention of ^{11}C-Pittsburgh compound B (^{11}C-PIB)[22, 23]. ^{11}C-PBB3 has been produced with sufficient radioactivity and high quality, demonstrating its clinical utility. Its radiosynthesis, photoisomerization, biodistribution and metabolites have also been studied [12]. Furthermore, a previous study showed that PBB3 could bind to tau fibrils in postmortem AD brain tissue [21]. Recently, a ^{18}F-labeled PBB3 derivative, ^{18}F-APN1607 (^{18}F-PM-PBB3) has been developed and demonstrated to improve imaging characteristics of ^{11}C-PBB3 with wider availability [24]. The structure of ^{18}F-PM-PBB3 had been reported and the results of biodistribution, metabolites and histo-pathological correlation in animal and human studies had been submitted[5]. In the present study, we applied the latest developed tracer (i.e.,^{18}F-APN1607) to evaluate the clinical and neuroimaging characteristics of tauopathies in AD patients and normal controls (NCs). We hypothesized that the ^{18}F-APN1607 tau PET tracer could effectively display the AD-associated regions with significant tau deposition and revealed the topographical patterns of cognitive changes.

Methods

Study rationale

An open-label study to evaluate the performance of a novel tau imaging tracer in AD patients and NCs was conducted. Participants were recruited from among patients and healthy volunteers residing in Taiwan. The study protocol was approved by the Chang Gung Memorial Hospital Institutional Review Board (CGMHIRB No. 201700982A0) and the Governmental Department of Health (1066060482). Written informed consent was obtained from all participants prior to the study procedure. All methods were performed in accordance with the relevant guidelines and regulations. Neurological examinations were performed on all participants. Each participant completed the following components: screening evaluation, brain magnetic resonance imaging (MRI), ^{18}F-AV-45 (florbetapir) PET and ^{18}F-APN1607 PET. The screening procedures included vital signs, electrocardiography (ECG), physical examinations and laboratory tests. In addition, ^{18}F-AV-45 PET imaging results were used as part of the inclusion criteria to confirm the presence and absence of amyloid deposition in patients with probable AD and in NCs. All participants completed a series of clinical assessments and clinical safety studies to ensure that they were medically stable after participating in this study. A final follow-up phone call for adverse event assessment was made within 7 days following ^{18}F-APN1607 PET imaging. There were no

adverse or clinically detectable pharmacologic effects in any participant. No significant changes in vital signs or the results of laboratory studies or ECG were observed, either.

Subjects

A total of twenty-two participants comprising twelve NC and ten patients with probable AD were included in this study. Neuropsychological assessments, including the Mini-Mental State Examination (MMSE), the Clinical Dementia Rating (CDR) scale and the cognitive subscale of the Alzheimer's Disease Assessment Scale (ADAS-cog) with greater scores referring to worse cognition, were administered to all participants[25-27]. The CDR sum of box scores (CDR-SB) was used for disease severity. Participants with a diagnosis of mild to moderate probable AD (CDR = 0.5 to 2.0 or MMSE = 10-28) ranged in age from 50 to 90 years old, and were required to have positive ^{18}F-AV-45 PET imaging results and to fulfill the National Institute for Neurological and Communicative Disorders and Stroke-Alzheimer's Disease and Related Disorder Association (NINCDS-ADRDA) criteria[28]. The presence of the ε2, ε3, and ε4 alleles of the apolipoprotein E gene (ApoE) was determined by assessing the sequences at two single-nucleotide polymorphisms (SNPs; rs429358 and rs7412)[29]. NCs in the study were required to be 20-90 years old with normal cognitive function (CDR = 0 or MMSE = 26-30, Wechsler Logical Memory score > 5) and negative ^{18}F-AV-45 PET results.

Image acquisition

^{18}F-APN1607 was prepared and synthesized at the cyclotron facility of Chang Gung Memorial Hospital[30]. All participants were studied in a Biograph mCT PET/computed tomography system (Siemens Medical Solutions, Malvern, PA, USA) and underwent MRI to screen for other diseases (e.g., hemorrhages and structural lesions) and perform spatial normalization with PET images. Brain MRI was acquired on a 3 T Siemens Magnetom TIM Trio scanner (Siemens Medical Solutions) for detailed anatomical images. High-resolution T1-weighted images were acquired with the following parameters: TR/TE: 2000/2.63 milliseconds; NEX: 1; voxel size: 1.0×1.0×1.0 mm^3. FLAIR: TR/TE: 10000/94 milliseconds, IR: 2500 milliseconds, NEX: 2, voxel size: 0.47×0.47×5 mm^3. For the ^{18}F-APN1607 PET study, a 10min scan was acquired after pseudo-equilibrium in the brain was reached at 90 min post-injection of 378 ± 11 MBq of ^{18}F-APN1607 [31]. The PET images were then reconstructed using a 3-D ordered-subset expectation maximization algorithm (4 iterations, 24 subsets; Gaussian filter: 2 mm; zoom: 3) with computed tomography–based attenuation correction and with the scatter and random correction procedures provided by the manufacturer. The reconstructed images had a matrix size of 400 × 400 × 148 and a voxel size of 0.68 × 0.68 × 1.5 mm^3. ^{18}F-AV-45 PET scans were performed one month before the ^{18}F-APN1607 PET scans. The ^{18}F-AV-45 radiosynthesis and PET data acquisition were performed according to our previous protocols[32, 33]. Briefly, all participants underwent ^{18}F-AV-45 PET scans on a Biograph mCT PET/CT System. PET images were acquired after intravenous injection of 374 ± 21 MBq of ^{18}F-AV-45. A 10 min scan was acquired starting at 50 mins after the tracer injection. PET images were reconstructed using the same method described above, and the images were then reconstructed with a matrix size of 400 × 400 × 148 and a voxel size of 0.68 × 0.68 × 1.5 mm^3.

Image analysis

All imaging data were transformed into the *N*euroimaging *I*n*f*ormatics *T*echnology *I*nitiative (NIFTI) format using the MRIcron tool (http://www.mccauslandcenter.sc.edu/mricro/mricron/) for further processing. For each participant, PET images (both ^{18}F-AV-45 and ^{18}F-APN1607 images) and T1-weighted images in native space were analyzed. We coregistrated each PET image to individual MRI using the SPM12 toolbox (http://www.fil.ion.ucl.ac.uk/spm/software/spm12/)[34]. This procedure ensured the ^{18}F-AV-45 PET and ^{18}F-APN1607 images in alignment with the native MR images. The Muller-Gartner method was used for partial volume correction[35]. Then, the high-resolution MR images in native space were normalized to the Montreal Neurological Institute (MNI) standard space with the DARTEL toolbox in SPM12 [36]. This transform matrix was applied to PET images. The averaged intensity across the whole cerebellum was used as the reference for the ^{18}F-AV-45 PET images, and the cerebellum gray matter considered having no amyloid and tau pathology in AD was used as the reference region for the ^{18}F-APN1607 PET images [37]. Eighteen regions of interest (ROIs), including the bilateral frontal, parietal, temporal, occipital lobes, anterior and posterior cingulate gyrus, precuneus, hippocampus, and the parahippocampus were selected based on the Harvard-Oxford cortical structural atlas, and the average values from both sides were used for further study[38]. Finally, the regional standardized uptake value ratios (SUVRs) from both ^{18}F-AV-45 PET images and ^{18}F-APN1607 PET images were calculated using the mean intensity in the target ROIs divided by the averaged intensity of the corresponding reference regions[39]. Analysis of gray matter (GM) volume was performed on T1-weighted MRI using the Computational Anatomy Toolbox (CAT), and comparison of two groups were performed to search for significant atrophic regions (http://www.neuro.uni-jena.de/cat/index.html#About)[40]. To study the regional GM atrophy in patients with AD and NCs, we firstly calculated the modulate GM volumes in the target ROIs and divided by the individual total intra-cranial volume (ICV) as regional GM ratios. In NCs, the mean value from each regional GM ratio was treated as the benchmark to explore the relative atrophy in patients with AD and NCs. Finally, the regional atrophic ratio in each ROI was calculated using the formula: regional atrophic ratio = (mean regional GM ratio – individual regional GM ratio)/mean regional GM ratio.

Statistical analysis

All statistical analyses were performed using SPSS (version 21.0, Chicago, IL). Continuous variables were expressed as the mean ± standard deviation (SD). Nonparametric Mann–Whitney *U* tests and chi-squared/Fisher's exact tests were performed to compare age and gender distributions between AD patients and NCs. In the MRI study, a significant level of GM atrophy between the two groups was defined as an uncorrected p-value < 0.01 with a corresponding t-value > 2.54 and a cluster size > 100 voxels. For PET analysis, the effect sizes of Mann–Whitney *U* test of regional SUVRs in both ^{18}F-AV-45 PET images and ^{18}F-APN1607 PET images were measured by η^2 (range 0-1) as described in the previous literature [41, 42]. Pairwise correlation using Spearman's rho was used to study the associations of regional SUVRs between the ^{18}F-AV-45 PET images and the ^{18}F-APN1607 PET images. To study the associations between cognition and the regional SUVRs derived from the ^{18}F-AV-45 PET images and ^{18}F-APN1607 PET images, we performed regression analyses. To study the sequential changes of regional SUVRs in the ^{18}F-AV-45 PET images, ^{18}F-APN1607 PET images and regional atrophic ratio from MRI images, we applied a nonlinear curve fitting model using the software GraphPad Prism, version 5.0 (GraphPad Inc., San Diego, CA). Statistical significance was defined as a p-value < 0.01.

Results

Demography

The demographic information of the twelve participants with probable AD and ten NCs was described in Table 1. The mean age of patients with probable AD was older than that of NCs (mean age of probable AD patients: NCs = 75.2 ± 10.0: 56.0 ± 11.8, $p < 0.01$). The mean interval from disease onset to scanning time in patients with probable AD was 6.1 ± 2.4 years. No significant group differences in gender, ApoE4 genotype and total ICV differences were found ($p = 0.39$, $p = 0.63$ and $p = 0.19$, respectively). Significantly lower MMSE and higher ADAD-cog and CDR-SB scores were found in patients with probable AD than in NCs (all ps < 0.01). Nonparametric Mann–Whitney *U* tests revealed significantly lower GM ratios in the parietal, temporal, occipital, posterior cingulate gyrus, precuneus, hippocampus and parahippocampus of probable AD patients than those of NCs (all ps< 0.01, Supplementary table 1).

Visual description of ^{18}F-APN1607 PET images in probable AD patients and NCs

Figure 1A shows four representive cases of ^{18}F-APN1607 PET images in NC, and patients with probable AD with mild or moderate stages. Upon visual inspection of ^{18}F-APN1607 PET images in NCs, there were no prominent hyperintensities in the cortical regions (Figure 1B). The cerebral white matter, midbrain and basal ganglia also showed no significant uptake. In five of twelve NCs, the mean choroid plexus revealed approximately 2.5-5 times higher SUVRs than the reference regions. In patients with probable AD, the regions showing the most significantly increased uptake were the precuneus, the parietal, temporal, and frontal regions, and the parahippocampal region. The medial occipital region and the insular cortex showed weakly increased tracer uptake compared with the reference regions. The choroid plexus showed increased tracer uptake in seven of ten patients with probable AD. As for GM, patients with probable AD showed significant GM atrophy in the bilateral medial temporal, precuneus and parietal regions, a topographical distribution similar to that of tau deposition from averaging ^{18}F-APN1607 PET images of all patients with probable AD(Figure 1C-D).

Regional differences of SUVRs in ^{18}F-APN1607 and ^{18}F-AV-45 PET images

Nonparametric Mann–Whitney *U* tests were performed to study the regional differences in ^{18}F-APN1607 PET images between patients with probable AD and NCs. Table 2 shows that the frontal, parietal, temporal, and occipital lobes, the anterior and posterior cingulate gyrus, the precuneus, and the parahippocampal region had significantly higher SUVRs in probable AD patients than in NCs (all ps < 0.01). The effect sizes in all of the above regions were medium to large ($\eta^2 = 0.44 - 0.75$). The hippocampal region did not show a significant group difference ($p = 0.14$). In the ^{18}F-AV-45 PET imaging study, patients with AD showed significantly higher SUVRs in the frontal, parietal, temporal, and occipital lobes, the anterior and posterior cingulate gyri, and the precuneus region (all ps < 0.01). There were no significant group differences in the hippocampal and parahippocampal regions ($p = 0.08$ and 0.81, respectively). The effect size values from ^{18}F-AV-45 PET images were smaller than those from ^{18}F-APN1607 PET images in most regions. Table 3 shows the results of pairwise correlations of regional SUVRs derived from the ^{18}F-AV-45 PET images and the ^{18}F-APN1607 PET images. The values of Spearman's rho (rank-correlation coefficient) showed significant associations in the frontal, temporal, parietal, and occipital lobes, the anterior and posterior cingulate gyri, and the precuneus region. Interestingly, the SUVRs of the parahippocampus from the ^{18}F-APN1607 PET images had significant associations with those of all the above regions (all ps < 0.01), but the values from the ^{18}F-AV-45 PET images did not. The SUVRs from the

hippocampal region showed no significant associations with any of the regions. These results demonstrated that similar trends of the tau and amyloid depositions between the parahippocampus and the rest of the studied brain regions but the hippocampus failed to show the same pattern.

Correlation studies between regional SUVRs and clinical parameters

To explore the correlations between regional SUVRs and clinical scores in ^{18}F-APN1607 PET images, we performed regression analyses in patients with probable AD and in NCs. The SUVRs of the frontal, parietal, temporal, and occipital lobes, the anterior and posterior cingulate gyri, the precuneus, and the parahippocampal regions showed significant correlations with the ADAS-cog scores (all ps < 0.01). The values of R squared ranged from 0.54 to 0.68. The hippocampus did not show a significant association with the ADAS-cog scores ($p = 0.53$). Figure 2 shows the significant correlation between the regional SUVRs of the posterior cingulate gyrus and the ADAS-cog scores. Age, gender and ApoE4 gene were used as covariates in the regression model, and there were no significant associations with regional SUVRs ($p = 0.23$, $p = 0.67$ and $p = 0.85$, respectively).The CDR-SB showed significant associations with the above regions, and the values of R squared ranged from 0.52 to 0.61 (all ps < 0.01), except for the hippocampus regions ($p = 0.77$). In ^{18}F-AV-45 PET images, regional SUVRs of the frontal, parietal, temporal, and occipital lobes, the anterior and posterior cingulate gyri, and the precuneus region showed significant associations with the ADAS-cog scores (all ps < 0.01). The regional SUVRs from the parietal, temporal, and occipital lobes, the posterior cingulate gyrus, and the precuneus region showed significant associations with CDR-SB (all $p < 0.01$).

Relations between regional SUVRs in ^{18}F-APN1607 and ^{18}F-AV-45 PET images and cognitive status

To further explore the relationship between regional SUVRs in ^{18}F-APN1607 PET images and the ADAS-cog scores, we used the sigmoidal four-parameter logistic curve fitting model(Figure 3A). The SUVRs in the parahippocampal region rapidly increased values as the ADAS-cog scores increased and then reached a plateau. This was followed by increased SUVRs of the posterior cingulate gyrus and the temporal, frontal, parietal and occipital regions, whose values sequentially increased as the ADAS-cog scores increased (Figure 3B). Quantitative analysis indicated that the ADAS-cog scores at the inflection points of the sigmoidal curves from the above regions showed the lowest value in the parahippocampus (20.3), followed by the precuneus (38.6), temporal lobe (39.9), posterior cingulate gyrus (42.5), frontal lobe (42.5), parietal lobe (45.7), anterior cingulated gyrus (51.5) and occipital lobe (56). Figure 4 shows the combination of SUVRs from the ^{18}F-AV-45 and ^{18}F-APN1607 PET images and regional atrophic ratios in the different ROIs. In most regions, the SUVRs from the ^{18}F-AV-45 PET images rapidly increased as the ADAS-cog scores increased, except the parahippocampus region(Figure 4A), which didn't show increased uptake as the ADAS-cog scores increased. The SUVRs in most ROIs from the ^{18}F-APN1607 PET images showed gradual increases and reached plateaus as the ADAS-cog scores increased, except the occipital region. The regional atrophic ratios from T1-weighted MRI showed flatter curves of increase, compared with the curves from the ^{18}F-APN1607 PET images as the ADAS-cog scores increased, except the parahippocampus region.

Discussion

In the current work, we applied the most recently developed tau tracer, ^{18}F-APN1607, in a group of patients with probable AD and a group of NCs. Our study showed several advantages of this new tau tracer. First, this tracer revealed a clear background in the midbrain, basal ganglia and cerebral white matter regions in NCs. In patients with probable AD, the tracer demonstrated significantly increasing intensities in AD-associated cortical regions with medium to large effect sizes (mean effect size = 0.71 in the significant regions). Second, the regional SUVRs in AD-associated cortical regions showed significant correlations with the ADAS-cog scores and CDR-SB, suggesting that tau deposition correlated with clinical severity in vivo. Third, the pattern of sequentially increasing regional SUVRs from the ^{18}F-APN1607 PET images corresponding well with disease severity and hence revealed the topographical progression of tau distribution in AD. Finally, the combined ^{18}F-AV-45, ^{18}F-APN1607 PET and regional atrophic ratio information from the same region could support the hypothesis that amyloid deposition would reach a plateau earlier than tau deposition before neuronal degeneration revealed[43]. These results are in line with the pathological observations from different Braak stages of AD [20].

The characteristics of in vivo ^{18}F-APN1607 PET imaging

In vivo imaging of the deposition of tau proteins faced several inherent obstacles, such as the intracellular deposition of tau aggregates, the six different isoforms of tau, the similarity of the β-sheet structure between tau and many other misfolded proteins, and the colocalization of tau with 5-20 times its concentration in β-amyloid protein in GM areas[44]. Despite these challenges, several tau tracers have been synthesized in the past few years. The first-generation tracers (e.g., ^{18}F-THK-5317, ^{18}F-THK-5351, ^{18}FAV-1451 and ^{11}C-PBB3) have been extensively used in research studies. The second-generation compounds, namely, ^{18}F-MK-6240, ^{18}F-JNJ-64349311, ^{18}F-PI-2620, ^{18}F-GTP1, and ^{18}F-APN1607, have started to be used for in vivo studies[14, 45]. The advantages of the second- generation compounds include a lack of off-target binding in the basal ganglia and thalamus and a relatively low affinity for the enzyme MAO-B[46-48]. A directly head-to-head comparison between the first-generation and second-generation tau tracers also revealed that different molecular binding targets existed in these tracers[49]. In the current study, we showed that there is no significant uptake of the PET tracer ^{18}F-APN1607 in the midbrain or the basal ganglia. Similar studies results have been found using ^{11}C-PBB3 in healthy participants and using autoradiographic methods in human tissue[50, 51]. These tracers could be beneficial for research on various tau-related neurodegenerative diseases, such as progressive supranuclear palsy and corticobasal syndrome. Furthermore, the AD-associated cortical regions of subjects with probable AD showed significantly increased SUVRs in ^{18}F-APN1607 PET images, with medium to large effect size, which could be used to easily distinguish the abnormal cortical regions in clinical practice. In the current work, the tracer ^{18}F-APN1607 still had off-target binding in the choroid plexus in five of twelve NCs (42%) and in seven of ten participants with probable AD (70%). From a previous autoradiographic study using ^{18}F-THK-5351 or ^{18}F-AV-1451 in postmortem human brains, these first-generation tau tracers had strong binding properties in tissue with a high density of melanin-containing cells [51]. The compound ^{18}F-APN1607 may have similar characteristics. There are also other possible explanations that have been mentioned; for example, the epithelial cells of the choroid plexus contain tangle-like structures that could be labeled by ^{18}F-AV-1451, or the choroid plexus could act as a gatekeeper for the accumulation of tau protein[52, 53].

Significant associations between regional SUVRs in ^{18}F-APN1607 PET and clinical scores

In previous AD studies, cognitive decline and tau accumulation showed a close relationship [54-56]. Based on investigations using ^{18}F-AV-1451, Aschenbrenner et al. suggested that increasing levels of tau most consistently relate to declines in cognition in patients with AD[57]. In our results, SUVRs in ^{18}F-APN1607 PET images from AD-associated regions showed significantly positive correlations with the ADAS-cog scores and CDR-SB scores ($p < 0.01$), which demonstrated that increasing tau burden correlated with decreasing cognition and increasing disease severity. The SUVRs inAD-associated regions shown on^{18}F-AV-45 PET images also showed significant associations with the ADAS-cog scores and CDR-SB scores, which may be related to the small sample size in this study.

The sequential changes in regional SUVRs from ^{18}F-APN1607 PET imaging

The pathological study showed that the spread of tau deposits started from the entorhinal cortex (Braak stages I/II), moving to the inferolateral temporal cortex and parts of the medial parietal lobe (stages III/IV), and eventually spreading throughout the association cortex (V/VI)[20, 58]. Our results using in vivo ^{18}F-APN1607 PET images demonstrated a similar topographical pattern. At least three patterns of tau deposition could be found (Figure 3A). The first pattern was in the parahippocampal region; tau deposition rapidly increased and then reached a plateau (rapid saturation) as the ADAS-cog scores increased. The second pattern was in the posterior cingulate gyrus and the temporal, frontal and parietal regions, undergoing a slow progressive increase in tau deposits and then reaching to plateaus. The final pattern was in the occipital region, which showed a gradual increase of tau deposition without a plateau (Figure 3). The ADAS-cog scores at the inflection points of the sigmoidal curves showed the lowest value in the parahippocampus, followed by the precuneus, temporal lobe, posterior cingulate gyrus, frontal lobe, parietal lobe, anterior cingulated gyrus and occipital lobe. These findings were in agreement with the previous neuropathological evidence of neurofibrillary changes from transentorhinal stages to limbic stages and finally to neocortical stages[20].

The evolution of amyloid, tau and atrophic changes in different regions

In most of the ROIs, the evolution of SUVRs from ^{18}F-AV-45 and ^{18}F-APN1607 PET images and regional atrophic ratios showed that the amyloid burden usually rapidly increased to a plateau as the ADAS-cog scores increased, especially in the low ranges of ADAS-cog scores. The patterns of increasing tau deposition were regionally dependent. Finally, the regional atrophic ratios from MRI showed progressively increased values without plateaus (Figure 4).

When we combined the SUVRs from ^{18}F-AV-45 and ^{18}F-APN1607 PET images and regional atrophic ratio information in the same ROIs to explore the sequential changes, we found that the amyloid burden usually manifested earlier than tau deposition and tau deposition usually started earlier then regional atrophies in most regions (Figure 4). In the parahippocampal region, tau deposition and regional atrophic ratio rapidly increased in the low ADAS-cog scores range but the amyloid burden didn't show a significant increase(Figure 4A). On the other hand, the occipital region showed a progressive increase of tau deposition and regional atrophy without a plateau phase(Figure 4B). These findings may indicate that cerebral amyloid deposition reached a saturation state more rapidly than tau deposition and neurodegeneration in most areas, but this sequential change also had the regional variability. Currently, our findings from the cross-sectional data could demonstrate the importance of amyloid-tau-neurodegeneration (ATN) sequential changes in regional base level, which were

compatible with the widely hypothesized model of AD and ATN classification system in the AD research framework[59, 60].

Limitations

Several limitations of the current work need to be addressed. First, the tau tracer ^{18}F-APN1607 is a relatively new tracer, thus the pathological results are not yet available in our study. Up to now, only postmortem brain tissue had been studied with this tracer, and there have been no clinicopathological correlation studies using this tracer yet[21]. Furthermore, the six isoforms of tau in the brain include 3R and 4R tau, whose misfolding is responsible for various neurodegenerative diseases, such as progressive supranuclear palsy, corticobasal syndrome and frontotemporal dementia[61]. Whether the tau tracer ^{18}F-APN1607 can differentiate among all isoforms is an open question that needs further investigation. In addition, direct application of MAO-B inhibitors in patients undergoing ^{18}F-APN1607 PET imaging has not been performed, and it could be difficult to eliminate these concerns about the first-generation tau tracers[15]. Second, our study had a small sample size, a significant age difference between AD patients and NCs, and no participants with amnestic mild cognitive impairment. We acknowledge the demographic differences between groups, and we used age and gender as covariates to study the correlations of regional SUVRs from ^{18}F-APN1607 PET imaging with ADAS-cog and CDR-SB scores. Increasing the sample size and adding amnestic patients will help us explore the features of this tau tracer. Third, we used the ADAS-cog scores as the severity index for curve fitting with the regional SUVRs from ^{18}F-AV-45 , ^{18}F-APN1607 PET images and regional atrophy ratios. We acknowledge that any biomarker changes to be incorporated into the hypothetical model of AD should come from longitudinal studies rather than cross-sectional observations, and our findings must be interpreted conservatively. Future studies should focus on longitudinal changes in ^{18}F-APN1607 PET imaging with the aid of other biomarkers, which will may provide further evidence for the AD hypothetical model.

Conclusions

This is the first in vivo study of the PET tracer ^{18}F-APN1607 in patients with mild to moderate AD. Our findings suggest that ^{18}F-APN1607 PET imaging has a clear background and no off-target binding in the basal ganglia or the thalamus. The regional SUVRs of the AD-associated regions were significantly correlated with cognitive deficits and disease severity. Finally, combined tau imaging with information on amyloid deposition and neurodegeneration may further our understanding of dynamic biomarker changes in the regional base level during the progression of AD.

Abbreviations

AD: Alzheimer's disease; ADAS-cog: cognitive subscale of the Alzheimer’s Disease Assessment Scale; ApoE: apolipoprotein E gene; CDR: Clinical Dementia Rating; CDR-SB: CDR sum of box scores; ICV: intra-cranial volume; MAO-A: monoamine oxidase A; MAO-B: monoamine oxidase B; MMSE: Mini-Mental State Examination; MRI: magnetic resonance imaging; PET: positron emission tomography; SUVR: standardized uptake value ratio.

Declarations

Ethics approval and consent to participate: All procedures performed in studies involving human participants were in accordance with the ethical standards of the Chang Gung Memorial Hospital Institutional Review Board (CGMHIRB No. 201700982A0) and the Governmental Department of Health (1066060482) and with the 1964 Helsinki declaration and its later amendments or comparable ethical standards. Informed consent was obtained from all individual participants included in the study.

Consent for publication: All co-authors have read and approved the submission.

Availability of data and materials: The datasets used and/or analyzed in the current study are available from the corresponding author on reasonable request.

Competing interests: Ming-Kuei Jang, Tzu-Chen Yen and Makoto Higuchi own equity of APRINOIA Therapeutics. Other authors declare that he/she has no conflict of interest.

Funding: This study was funded/sponsored by APRINOIA Therapeutic Inc.

Authors' contributions: for the ideal generation(JLH, KJL,ITH,KLH),material preparation(KLH,CHL,HCW,YCW,CYH,TCY,MH,MKJ,CCH), analysis data and interpretation of the results, drafted manuscript and critical feedback and helped revising the paper(JLH,KJL,ITH,TCY,CCC). All authors read and approved the final manuscript.

Acknowledgements: We thank the patients and healthy individuals for their participation in this study.

References

1. Lee VM, Goedert M, Trojanowski JQ: **Neurodegenerative tauopathies**. *Annu Rev Neurosci* 2001, **24**:1121-1159.
2. McKee AC, Cantu RC, Nowinski CJ, Hedley-Whyte ET, Gavett BE, Budson AE, Santini VE, Lee HS, Kubilus CA, Stern RA: **Chronic traumatic encephalopathy in athletes: progressive tauopathy after repetitive head injury**. *J Neuropathol Exp Neurol* 2009, **68**(7):709-735.
3. Villemagne VL, Okamura N: **Tau imaging in the study of ageing, Alzheimer's disease, and other neurodegenerative conditions**. *Curr Opin Neurobiol* 2016, **36**:43-51.
4. Okamura N, Harada R, Ishiki A, Kikuchi A, Nakamura T, Kudo Y: **The development and validation of tau PET tracers: current status and future directions**. *Clin Transl Imaging* 2018, **6**(4):305-316.
5. Leuzy A, Chiotis K, Lemoine L, Gillberg PG, Almkvist O, Rodriguez-Vieitez E, Nordberg A: **Tau PET imaging in neurodegenerative tauopathies-still a challenge**. *Mol Psychiatry* 2019, **24**(8):1112-1134.
6. Xia CF, Arteaga J, Chen G, Gangadharmath U, Gomez LF, Kasi D, Lam C, Liang Q, Liu C, Mocharla VP *et al*: **[(18)F]T807, a novel tau positron emission tomography imaging agent for Alzheimer's disease**. *Alzheimers Dement* 2013, **9**(6):666-676.
7. Chien DT, Bahri S, Szardenings AK, Walsh JC, Mu F, Su MY, Shankle WR, Elizarov A, Kolb HC: **Early clinical PET imaging results with the novel PHF-tau radioligand [F-18]-T807**. *J Alzheimers Dis* 2013, **34**(2):457-468.
8. Harada R, Okamura N, Furumoto S, Furukawa K, Ishiki A, Tomita N, Hiraoka K, Watanuki S, Shidahara M, Miyake M *et al*: **[(18)F]THK-5117 PET for assessing neurofibrillary pathology in Alzheimer's disease**. *Eur J*

Nucl Med Mol Imaging 2015, **42**(7):1052-1061.

9. Stepanov V, Svedberg M, Jia Z, Krasikova R, Lemoine L, Okamura N, Furumoto S, Mitsios N, Mulder J, Langstrom B *et al*: **Development of [(11)C]/[(3)H]THK-5351 - A potential novel carbon-11 tau imaging PET radioligand**. *Nucl Med Biol* 2017, **46**:50-53.
10. Hsiao IT, Lin KJ, Huang KL, Huang CC, Chen HS, Wey SP, Yen TC, Okamura N, Hsu JL: **Biodistribution and Radiation Dosimetry for the Tau Tracer (18)F-THK-5351 in Healthy Human Subjects**. *J Nucl Med* 2017, **58**(9):1498-1503.
11. Betthauser TJ, Ellison PA, Murali D, Lao PJ, Barnhart TE, Furumoto S, Okamura N, Johnson SC, Engle JW, Nickles RJ *et al*: **Characterization of the radiosynthesis and purification of [(18)F]THK-5351, a PET ligand for neurofibrillary tau**. *Appl Radiat Isot* 2017, **130**:230-237.
12. Hashimoto H, Kawamura K, Igarashi N, Takei M, Fujishiro T, Aihara Y, Shiomi S, Muto M, Ito T, Furutsuka K *et al*: **Radiosynthesis, photoisomerization, biodistribution, and metabolite analysis of 11C-PBB3 as a clinically useful PET probe for imaging of tau pathology**. *J Nucl Med* 2014, **55**(9):1532-1538.
13. Walji AM, Hostetler ED, Selnick H, Zeng Z, Miller P, Bennacef I, Salinas C, Connolly B, Gantert L, Holahan M *et al*: **Discovery of 6-(Fluoro-(18)F)-3-(1H-pyrrolo[2,3-c]pyridin-1-yl)isoquinolin-5-amine ([(18)F]-MK-6240): A Positron Emission Tomography (PET) Imaging Agent for Quantification of Neurofibrillary Tangles (NFTs)**. *J Med Chem* 2016, **59**(10):4778-4789.
14. Declercq L, Rombouts F, Koole M, Fierens K, Marien J, Langlois X, Andres JI, Schmidt M, Macdonald G, Moechars D *et al*: **Preclinical Evaluation of (18)F-JNJ64349311, a Novel PET Tracer for Tau Imaging**. *J Nucl Med* 2017, **58**(6):975-981.
15. Ng KP, Pascoal TA, Mathotaarachchi S, Therriault J, Kang MS, Shin M, Guiot MC, Guo Q, Harada R, Comley RA *et al*: **Monoamine oxidase B inhibitor, selegiline, reduces (18)F-THK5351 uptake in the human brain**. *Alzheimers Res Ther* 2017, **9**(1):25.
16. Marquie M, Normandin MD, Vanderburg CR, Costantino IM, Bien EA, Rycyna LG, Klunk WE, Mathis CA, Ikonomovic MD, Debnath ML *et al*: **Validating novel tau positron emission tomography tracer [F-18]-AV-1451 (T807) on postmortem brain tissue**. *Ann Neurol* 2015, **78**(5):787-800.
17. Hostetler ED, Walji AM, Zeng Z, Miller P, Bennacef I, Salinas C, Connolly B, Gantert L, Haley H, Holahan M *et al*: **Preclinical Characterization of 18F-MK-6240, a Promising PET Tracer for In Vivo Quantification of Human Neurofibrillary Tangles**. *J Nucl Med* 2016, **57**(10):1599-1606.
18. Huang KL, Hsu JL, Lin KJ, Chang CH, Wu YM, Chang TY, Chang YJ, Liu CH, Ho MY, Wey SP *et al*: **Visualization of ischemic stroke-related changes on (18)F-THK-5351 positron emission tomography**. *EJNMMI Res* 2018, **8**(1):62.
19. Lee H, Seo S, Lee SY, Jeong HJ, Woo SH, Lee KM, Lee YB, Park KH, Heo JH, Yoon CW *et al*: **[18F]-THK5351 PET Imaging in Patients With Semantic Variant Primary Progressive Aphasia**. *Alzheimer Dis Assoc Disord* 2018, **32**(1):62-69.
20. Braak H, Braak E: **Neuropathological stageing of Alzheimer-related changes**. *Acta Neuropathol* 1991, **82**(4):239-259.
21. Ono M, Sahara N, Kumata K, Ji B, Ni R, Koga S, Dickson DW, Trojanowski JQ, Lee VM, Yoshida M *et al*: **Distinct binding of PET ligands PBB3 and AV-1451 to tau fibril strains in neurodegenerative tauopathies**. *Brain* 2017, **140**(3):764-780.

22. Maruyama M, Shimada H, Suhara T, Shinotoh H, Ji B, Maeda J, Zhang MR, Trojanowski JQ, Lee VM, Ono M *et al*: **Imaging of tau pathology in a tauopathy mouse model and in Alzheimer patients compared to normal controls**. *Neuron* 2013, **79**(6):1094-1108.
23. Wood H: **Alzheimer disease: [11C]PBB3--a new PET ligand that identifies tau pathology in the brains of patients with AD**. *Nat Rev Neurol* 2013, **9**(11):599.
24. Shimada H, Ono M, Tagai K, Kubota M, Kitamura S, Takuwa H, Seki C, Kimura Y, Ichise M, Shinotoh H *et al*: **Preclinical and clinical characterization of 18F-PM-PBB3, a PET ligand for diverse Tau pahtologies**. *Alzheimer's & Dementia: The Journal of the Alzheimer's Association* 2018, **14**(7):P318-P319.
25. Doraiswamy PM, Krishen A, Stallone F, Martin WL, Potts NL, Metz A, DeVeaugh-Geiss J: **Cognitive performance on the Alzheimer's Disease Assessment Scale: effect of education**. *Neurology* 1995, **45**(11):1980-1984.
26. Folstein MF, Folstein SE, McHugh PR: **"Mini-mental state". A practical method for grading the cognitive state of patients for the clinician**. *J Psychiatr Res* 1975, **12**(3):189-198.
27. Hughes CP, Berg L, Danziger WL, Coben LA, Martin RL: **A new clinical scale for the staging of dementia**. *Br J Psychiatry* 1982, **140**:566-572.
28. McKhann G, Drachman D, Folstein M, Katzman R, Price D, Stadlan EM: **Clinical diagnosis of Alzheimer's disease: report of the NINCDS-ADRDA Work Group under the auspices of Department of Health and Human Services Task Force on Alzheimer's Disease**. *Neurology* 1984, **34**(7):939-944.
29. Liao YC, Lee WJ, Hwang JP, Wang YF, Tsai CF, Wang PN, Wang SJ, Fuh JL: **ABCA7 gene and the risk of Alzheimer's disease in Han Chinese in Taiwan**. *Neurobiol Aging* 2014, **35**(10):2423 e2427-2423 e2413.
30. Hitoshi Shimada MO, Kenji Tagai, Manabu Kubota, Soichiro Kitamura, Hiroyuki Takuwa, Chie Seki, Yasuyuki Kimura, Masanori Ichise, Hitoshi Shinotoh, Keisuke Takahata, Naoyoshi Yamamoto, Yasunori Sano, Yuhei Takado, Paul Tempest, Ming-Kuei Jang, John Seibyl, Olivier Barret, David Alagille, Kenneth Marek, Naruhiko Sahara, Kazunori Kawamura, Ming-Rong Zhang, Tetsuya Suhara, Makoto Higuchi: **PRECLINICAL AND CLINICAL CHARACTERIZATION OF ^{18}F-PM-PBB3, A PET LIGAND FOR DIVERSE TAU PATHOLOGIES**. *Alzheimer's & Dementia: Journal of the Alzheimer's Association* 2018, **14**(7, supplement):318-319.
31. Huang C-C, Hsiao I-T, Lin K-J, Lian C-F, Hsu J-L, Huang K-L: **Optimal scanning time for the novel tau PET Tracer 18F-APN-1607**. *13th Human Amyloid Imaging* 2019:P392.
32. Lin KJ, Hsu WC, Hsiao IT, Wey SP, Jin LW, Skovronsky D, Wai YY, Chang HP, Lo CW, Yao CH *et al*: **Whole-body biodistribution and brain PET imaging with [18F]AV-45, a novel amyloid imaging agent--a pilot study**. *Nucl Med Biol* 2010, **37**(4):497-508.
33. Hsiao IT, Huang CC, Hsieh CJ, Wey SP, Kung MP, Yen TC, Lin KJ: **Perfusion-like template and standardized normalization-based brain image analysis using 18F-florbetapir (AV-45/Amyvid) PET**. *Eur J Nucl Med Mol Imaging* 2013, **40**(6):908-920.
34. Ashburner J, Friston KJ: **Unified segmentation**. *Neuroimage* 2005, **26**(3):839-851.
35. Gonzalez-Escamilla G, Lange C, Teipel S, Buchert R, Grothe MJ, Alzheimer's Disease Neuroimaging I: **PETPVE12: an SPM toolbox for Partial Volume Effects correction in brain PET - Application to amyloid imaging with AV45-PET**. *Neuroimage* 2017, **147**:669-677.
36. Ashburner J: **A fast diffeomorphic image registration algorithm**. *Neuroimage* 2007, **38**(1):95-113.

37. Scholl M, Lockhart SN, Schonhaut DR, O'Neil JP, Janabi M, Ossenkoppele R, Baker SL, Vogel JW, Faria J, Schwimmer HD *et al*: **PET Imaging of Tau Deposition in the Aging Human Brain**. *Neuron* 2016, **89**(5):971-982.

38. Frazier JA, Chiu S, Breeze JL, Makris N, Lange N, Kennedy DN, Herbert MR, Bent EK, Koneru VK, Dieterich ME *et al*: **Structural brain magnetic resonance imaging of limbic and thalamic volumes in pediatric bipolar disorder**. *Am J Psychiatry* 2005, **162**(7):1256-1265.

39. Joshi AD, Pontecorvo MJ, Clark CM, Carpenter AP, Jennings DL, Sadowsky CH, Adler LP, Kovnat KD, Seibyl JP, Arora A *et al*: **Performance characteristics of amyloid PET with florbetapir F 18 in patients with alzheimer's disease and cognitively normal subjects**. *J Nucl Med* 2012, **53**(3):378-384.

40. C. Gaser RD: **CAT - A Computational Anatomy Toolbox for the Analysis of Structural MRI Data**. In: *Human Brain Mapping*. 2016.

41. Sawilowsky SS: **"New Effect Size Rules of Thumb,"**. *Journal of Modern Applied Statistical Methods* 2009, **8**(2):467-474.

42. Fritz CO, Morris PE, Richler JJ: **Effect size estimates: current use, calculations, and interpretation**. *J Exp Psychol Gen* 2012, **141**(1):2-18.

43. Mouiha A, Duchesne S, Alzheimer's Disease Neuroimaging I: **Toward a dynamic biomarker model in Alzheimer's disease**. *J Alzheimers Dis* 2012, **30**(1):91-100.

44. Villemagne VL, Okamura N: **In vivo tau imaging: obstacles and progress**. *Alzheimers Dement* 2014, **10**(3 Suppl):S254-264.

45. Pascoal TA, Shin M, Kang MS, Chamoun M, Chartrand D, Mathotaarachchi S, Bennacef I, Therriault J, Ng KP, Hopewell R *et al*: **In vivo quantification of neurofibrillary tangles with [(18)F]MK-6240**. *Alzheimers Res Ther* 2018, **10**(1):74.

46. Victor Villemagne, Vincent Dore, Rachel Mulligan, Fiona Lamb, Pierrick Bourgeat, Olivier Salvado, and CM, Rowe C: **Evaluation of 18F-PI-2620, a second-generation selective tau tracer for the assessment of Alzheimer's and non-Alzheimer's tauopathies**. *Journal of Nuclear Medicine* 2018, **59**:410.

47. Aguero C, Dhaynaut M, Normandin MD, Amaral AC, Guehl NJ, Neelamegam R, Marquie M, Johnson KA, El Fakhri G, Frosch MP *et al*: **Autoradiography validation of novel tau PET tracer [F-18]-MK-6240 on human postmortem brain tissue**. *Acta Neuropathol Commun* 2019, **7**(1):37.

48. Murugan NA, Chiotis K, Rodriguez-Vieitez E, Lemoine L, Agren H, Nordberg A: **Cross-interaction of tau PET tracers with monoamine oxidase B: evidence from in silico modelling and in vivo imaging**. *Eur J Nucl Med Mol Imaging* 2019.

49. Chiotis K, Stenkrona P, Almkvist O, Stepanov V, Ferreira D, Arakawa R, Takano A, Westman E, Varrone A, Okamura N *et al*: **Dual tracer tau PET imaging reveals different molecular targets for (11)C-THK5351 and (11)C-PBB3 in the Alzheimer brain**. *Eur J Nucl Med Mol Imaging* 2018, **45**(9):1605-1617.

50. Perez-Soriano A, Arena JE, Dinelle K, Miao Q, McKenzie J, Neilson N, Puschmann A, Schaffer P, Shinotoh H, Smith-Forrester J *et al*: **PBB3 imaging in Parkinsonian disorders: Evidence for binding to tau and other proteins**. *Mov Disord* 2017, **32**(7):1016-1024.

51. Tago T, Toyohara J, Harada R, Furumoto S, Okamura N, Kudo Y, Takahashi-Fujigasaki J, Murayama S, Ishii K: **Characterization of the binding of tau imaging ligands to melanin-containing cells: putative off-target-binding site**. *Ann Nucl Med* 2019.

52. Ikonomovic MD, Abrahamson EE, Price JC, Mathis CA, Klunk WE: **[F-18]AV-1451 positron emission tomography retention in choroid plexus: More than "off-target" binding**. *Ann Neurol* 2016, **80**(2):307-308.
53. Raha-Chowdhury R, Henderson JW, Raha AA, Vuono R, Bickerton A, Jones E, Fincham R, Allinson K, Holland A, Zaman SH: **Choroid Plexus Acts as Gatekeeper for TREM2, Abnormal Accumulation of ApoE, and Fibrillary Tau in Alzheimer's Disease and in Down Syndrome Dementia**. *J Alzheimers Dis* 2019.
54. Ossenkoppele R, Schonhaut DR, Scholl M, Lockhart SN, Ayakta N, Baker SL, O'Neil JP, Janabi M, Lazaris A, Cantwell A *et al*: **Tau PET patterns mirror clinical and neuroanatomical variability in Alzheimer's disease**. *Brain* 2016, **139**(Pt 5):1551-1567.
55. Johnson KA, Schultz A, Betensky RA, Becker JA, Sepulcre J, Rentz D, Mormino E, Chhatwal J, Amariglio R, Papp K *et al*: **Tau positron emission tomographic imaging in aging and early Alzheimer disease**. *Ann Neurol* 2016, **79**(1):110-119.
56. Ossenkoppele R, Smith R, Ohlsson T, Strandberg O, Mattsson N, Insel PS, Palmqvist S, Hansson O: **Associations between tau, Abeta, and cortical thickness with cognition in Alzheimer disease**. *Neurology* 2019, **92**(6):e601-e612.
57. Aschenbrenner AJ, Gordon BA, Benzinger TLS, Morris JC, Hassenstab JJ: **Influence of tau PET, amyloid PET, and hippocampal volume on cognition in Alzheimer disease**. *Neurology* 2018, **91**(9):e859-e866.
58. Lowe VJ, Wiste HJ, Senjem ML, Weigand SD, Therneau TM, Boeve BF, Josephs KA, Fang P, Pandey MK, Murray ME *et al*: **Widespread brain tau and its association with ageing, Braak stage and Alzheimer's dementia**. *Brain* 2018, **141**(1):271-287.
59. Jack CR, Jr., Knopman DS, Jagust WJ, Petersen RC, Weiner MW, Aisen PS, Shaw LM, Vemuri P, Wiste HJ, Weigand SD *et al*: **Tracking pathophysiological processes in Alzheimer's disease: an updated hypothetical model of dynamic biomarkers**. *Lancet Neurol* 2013, **12**(2):207-216.
60. Jack CR, Jr., Bennett DA, Blennow K, Carrillo MC, Dunn B, Haeberlein SB, Holtzman DM, Jagust W, Jessen F, Karlawish J *et al*: **NIA-AA Research Framework: Toward a biological definition of Alzheimer's disease**. *Alzheimers Dement* 2018, **14**(4):535-562.
61. Choi Y, Ha S, Lee YS, Kim YK, Lee DS, Kim DJ: **Development of tau PET Imaging Ligands and their Utility in Preclinical and Clinical Studies**. *Nucl Med Mol Imaging* 2018, **52**(1):24-30.

Tables

Table 1. Demographic descriptions of probable AD patients and NCs.

	Probable AD (N = 10)	NCs (N = 12)	p-value
Mean age (years)	72.5 ± 10.0	56.0 ± 11.8	< 0.01
Gender (M:F)	4:6	7:5	0.39
Education (years)	10.2 ± 3.5	14.4 ± 4.3	0.03
Onset to scan time (years)	6.1 ± 2.4	-	-
Mean MMSE	12.5 ± 8.9	29.3 ± 0.9	< 0.01
Mean ADAS-cog	51.3 ± 21.8	7.2 ± 4.3	< 0.01
Mean CDR-SB	7.4 ± 4.6	0 ± 0	< 0.01
ApoE4 genotype (positive: negative)	4:5	2:5	0.63
Mean cortical SUVRs of ^{18}F-AV-45	1.41 ± 0.20	1.09 ± 0.04	< 0.01
Total ICV (ml)	1466.14 ± 160.61	1384.21 ± 111.72	0.19

AD: Alzheimer's disease; NC: normal control; MMSE: Mini-Mental State Examination; ADAS-cog: Alzheimer's Disease Assessment Scale cognitive subscale; ApoE: apolipoprotein E; CDR-SB: Clinical Dementia Rating scale sum of box scores; ICV: intra-cranial volume; SUVR: standardized uptake value ratio.

Table 2. Comparison of regional SUVRs from ^{18}F-APN1607 and ^{18}F-AV-45 PET imaging between probable AD patients and NCs.

	Mean cortical SUVRs of ^{18}F-APN1607 (mean ± SE)				Mean cortical SUVRs of ^{18}F-AV-45 (mean ± SE)			
Regions	Probable AD	NCs	p-value	Effect size (η^2)	Probable AD	NCs	p-value	Effect size (η^2)
Frontal	1.89 ± 0.19	0.86 ± 0.18	< 0.01	0.69	1.64 ± 0.08	1.01 ± 0.07	< 0.01	0.58
Parietal	1.62 ± 0.15	0.94 ± 0.14	< 0.01	0.74	1.63 ± 0.08	1.02 ± 0.07	< 0.01	0.65
Temporal	2.46 ± 0.20	0.99 ± 0.18	< 0.01	0.75	1.64 ± 0.08	1.06 ± 0.07	< 0.01	0.65
Occipital	2.42 ± 0.25	0.97 ± 0.23	< 0.01	0.75	1.59 ± 0.07	0.97 ± 0.06	< 0.01	0.71
Anterior cingulate gyrus	1.62 ± 0.15	0.94 ± 0.14	< 0.01	0.44	1.76 ± 0.09	1.17 ± 0.08	< 0.01	0.58
Posterior cingulate gyrus	2.63 ± 0.23	1.02 ± 0.21	< 0.01	0.75	1.95 ± 0.08	1.13 ± 0.08	< 0.01	0.63
Precuneus	2.67 ± 0.30	0.98 ± 0.28	< 0.01	0.75	1.86 ± 0.09	1.05 ± 0.07	< 0.01	0.68
Hippocampus	1.90 ± 0.24	1.47 ± 0.22	0.141	0.10	0.95 ± 0.04	1.06 ± 0.04	0.08	0.15
Parahippocampus	2.06 ± 0.15	0.97 ± 0.14	< 0.01	0.52	0.93 ± 0.05	0.96 ± 0.04	0.81	0.01

AD: Alzheimer’s disease; NC: normal control; SE: standard error; SUVR: standardized uptake value ratio.

Table 3. Pairwise correlation of regional SUVRs between ^{18}F-AV-45 PET imaging (rows) and ^{18}F-APN1607 PET imaging (columns).

Regions	Frontal	Parietal	Temporal	Occipital	Anterior cingulate gyrus	Posterior cingulate gyrus	Precuneus	Hippocampus	Parahippocampus
Frontal	0.82**	0.75**	0.73**	0.77**	0.75**	0.73**	0.77**	-0.26	0.17
Parietal	0.79**	0.74**	0.69**	0.75**	0.71**	0.70**	0.76**	-0.39	0.08
Temporal	0.73**	0.67**	0.65**	0.70**	0.64**	0.64**	0.69**	-0.29	0.05
Occipital	0.78**	0.75**	0.67**	0.77**	0.72**	0.70**	0.73**	-0.39	0.10
Anterior cingulate gyrus	0.64**	0.59**	0.49	0.63**	0.65**	0.56**	0.61**	-0.15	0.16
Posterior cingulate gyrus	0.86**	0.83**	0.75**	0.86**	0.81**	0.83**	0.88**	-0.41	0.21
Precuneus	0.86**	0.82**	0.75**	0.86**	0.78**	0.79**	0.85**	-0.41	0.19
Hippocampus	0.41	0.48	0.47	0.41	0.44	0.37	0.44	0.11	0.28
Parahippocampus	0.65**	0.58**	0.56**	0.61**	0.61**	0.53	0.63**	-0.19	0.14

SUVR: standardized uptake value ratio.

Spearman's rho (rank correlation coefficient) values; **: $p < 0.01$.

Figures

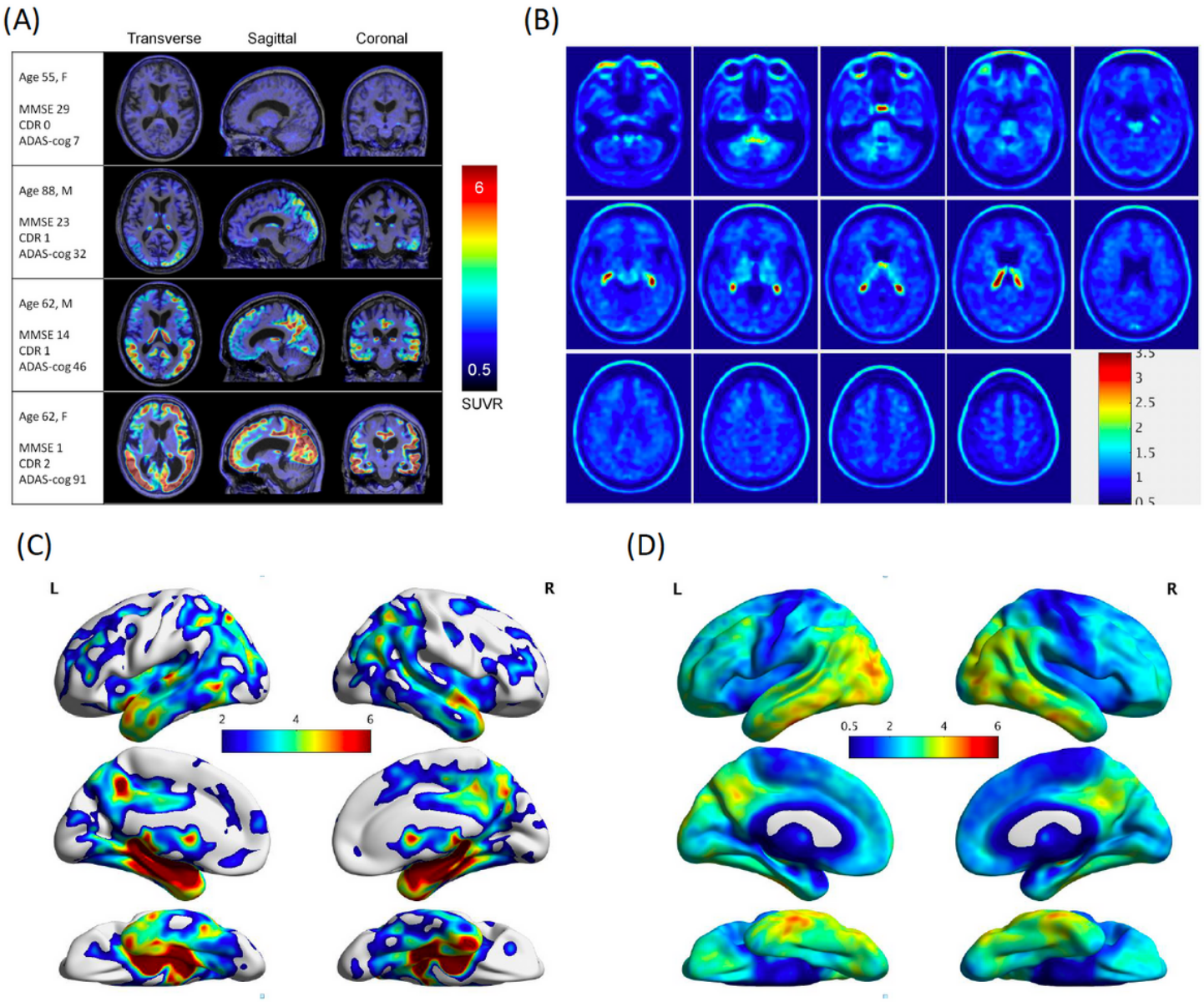

Figure 1

Four reprehensive cases of 18F-APN1607 PET images overlaid with T1 MRI images on three orthogonal views and the gray matter atrophy in patients with probable AD. (A). A 55 years old NC female had MMSE score = 29, CDR = 0 and ADAS-cog score = 7. A 88 years old male with probable AD, his MMSE score was 23, CDR = 1 and ADAS-cog score was 32. The inferior temporal and parietal regions showed increased SUVR values. The coronal view showed an increased uptake in choroid plexus region. A 62 years old male with probable AD, his MMSE score was 14, CDR = 1 and ADAS-cog score was 46. Compared with previous case, the lateral temporal, the posterior cingulate and the frontal regions showed increased SUVR values. A 62 years old female with probable AD, her MMSE score was 1, CDR = 2 and ADAS-cog score was 91. Extensively increase SUVR values in diffuse cortical regions were noted. Colormap represents SUVR values. (B). 3D surface projection view of significantly atrophic regions of GM in probable AD patients compared to NCs. Colormap represents significant Z-values. (C). 3D surface projection view of SUVRs from averaging all 18F-APN1607 PET images in patients with probable AD. Colormap represents SUVR values.

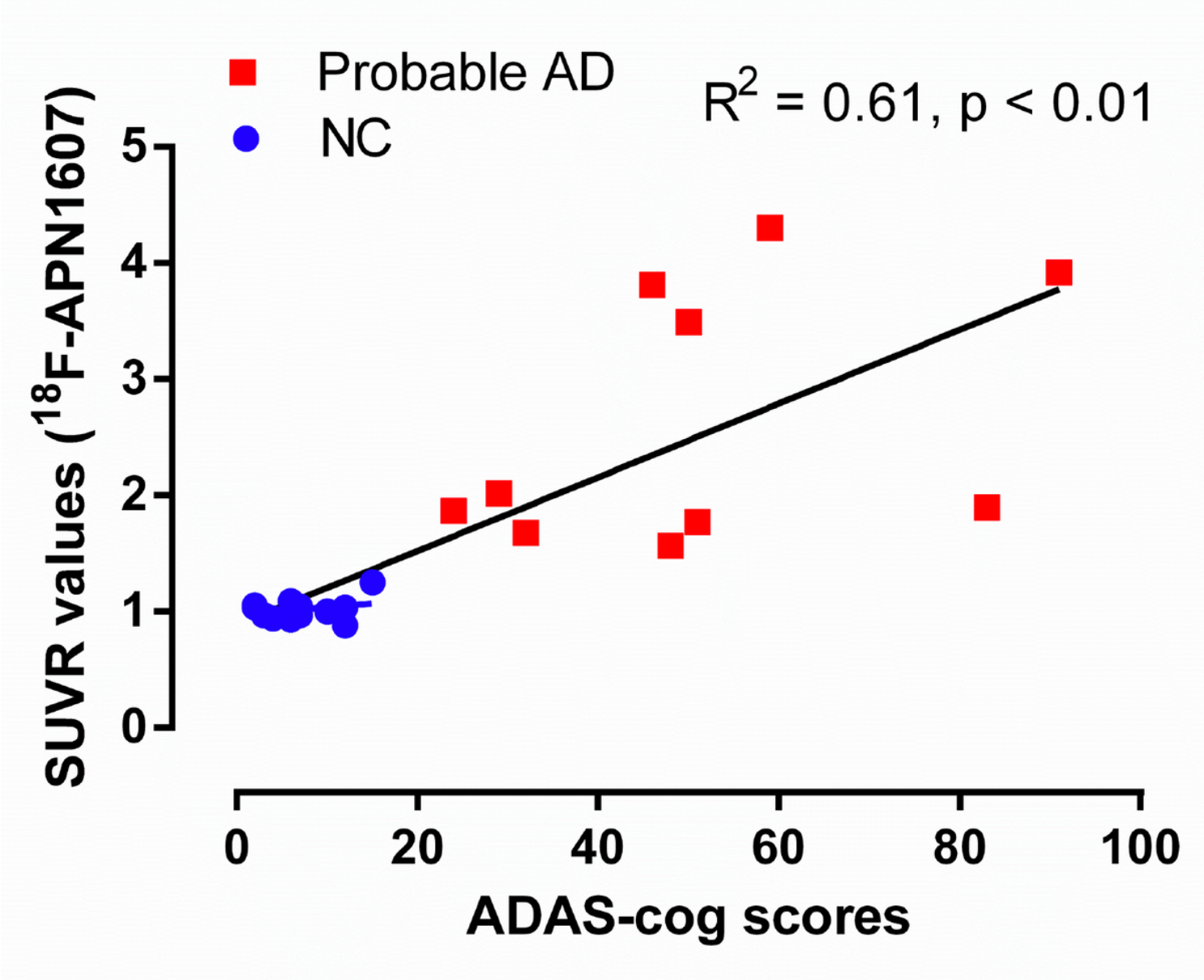

Figure 2

Significant correlation between the ADAS-cog scores and regional SUVRs determined from 18F-APN1607 PET images of the posterior cingulate gyrus.

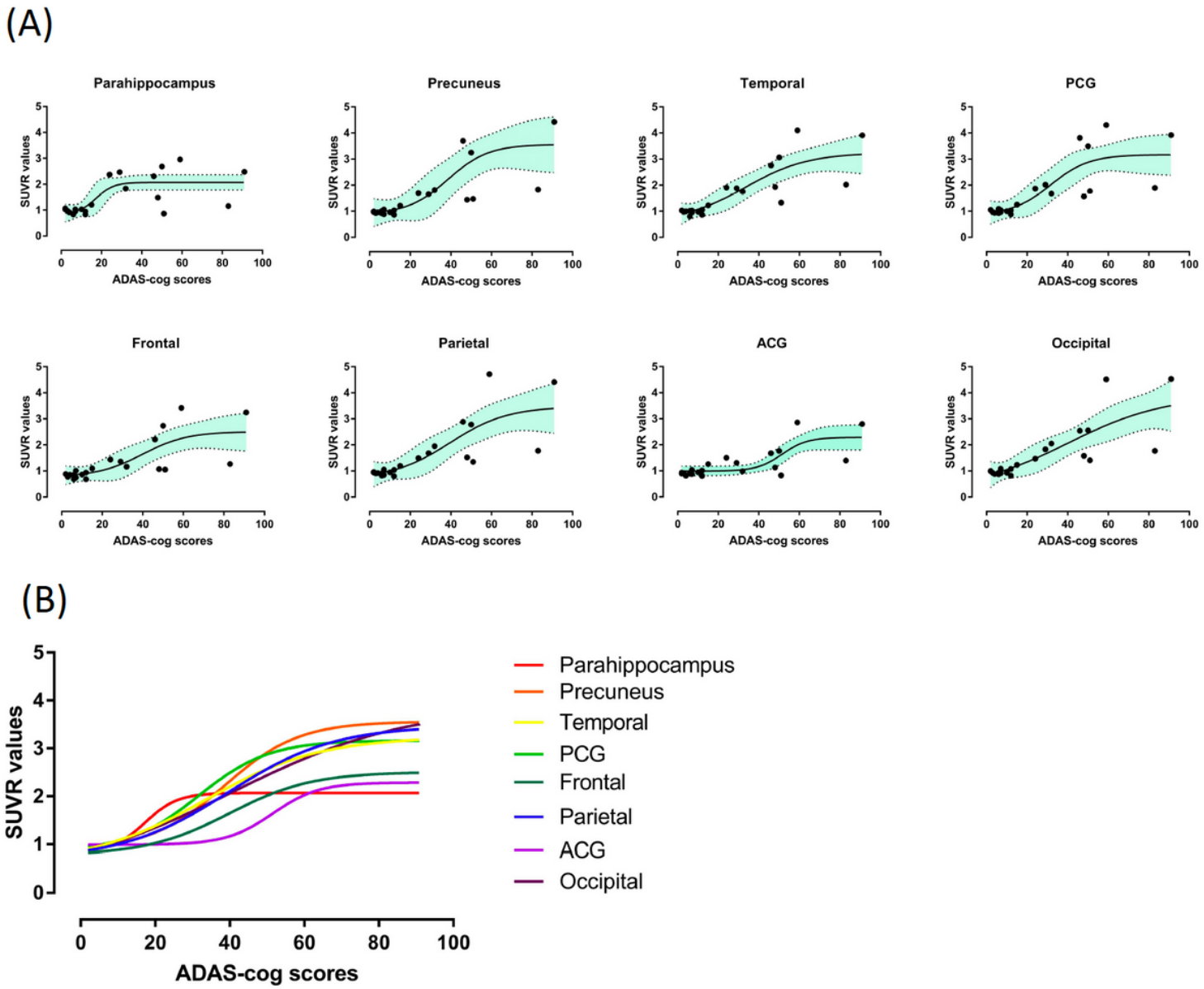

Figure 3

Sequentially increased regional SUVRs in 18F-APN1607 PET images from patients with probable AD. (A). Logistic curve fitting method was applied to the SUVRs of the parahippocampus, precuneus, temporal, posterior cingulate gyrus, frontal, parietal, the anterior cingulated gyrus and the occipital regions as the ADAS-cog scores increased. The blue area showed the 95% confidence interval area. The solid lines showed the mean fitting curves. (B). Combined fitting curves from all above regions showed the parahippocampal region had rapid saturation as the ADAS-cog scores increased, while the cingulate gyrus and the temporal, frontal, parietal regions showed sigmoidally increasing uptake. The occipital region showed gradually increasing uptake without a plateau.

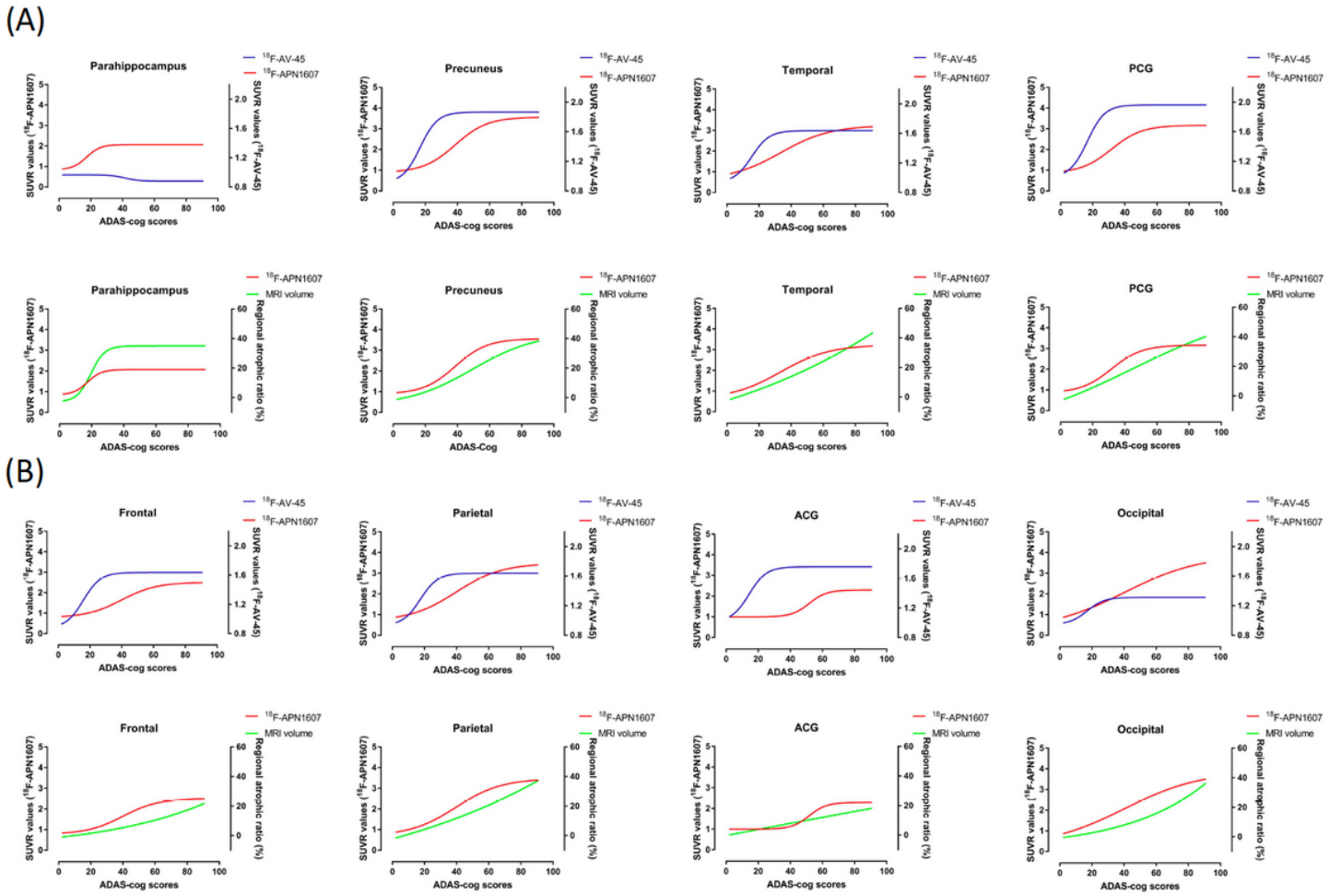

Figure 4

The evolution of increased SUVRs from 18F-AV-45 PET, 18F-APN1607 PET imaging and regional atrophic ratios in (A) the parahippocampus, the precuneus, the temporal and the posterior cingulated gyrus region and (B) the frontal, the parietal, the anterior cingulate gyrus and the occipital region. The SUVRs of 18F-AV-45 PET and 18F-APN1607 PET and regional atrophic ratios were fit for the ADAS-cog scores. In most regions, the amyloid burden showed rapid saturation as the ADAS-cog scores increased, while uptake associated with tau depositions were slowly increased. Finally, the regional atrophic ratios were gradually increased. ACG: anterior cingulated gyrus; PCG:posterior cingulated gyrus.

Supplementary Files

This is a list of supplementary files associated with this preprint. Click to download.

- Additionalfile1.docx